Icarus 403 (2023) 115648

Contents lists available at ScienceDirect

Icarus

journal homepage: www.elsevier.com/locate/icarus

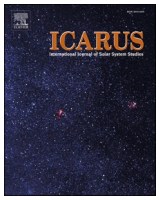

Ice dynamic recrystallization within Europa's ice shell: Implications for solid-state convection

Giuseppe Mitri [a,b,*]

[a] International Research School of Planetary Sciences, Pescara, Italy
[b] Dipartimento di Ingegneria e Geologia, Università d'Annunzio, Pescara, Italy

ARTICLE INFO

Keywords:
Europa
Solid-state convection
Ice rheology
Tidal dissipation
Ice dynamic recrystallization

ABSTRACT

Solid-state convection has been proposed to occur within Europa's ice shell based both on the interpretation of observed geological activity during Galileo spacecraft exploration and theoretical investigations. Laboratory experiments have investigated the effect of grain size insensitive creep and grain size sensitive creep on the ductile behaviour of polycrystalline ice. The ice grain size and the ice impurities content and, consequently, the viscosity of the ice within Europa's ice shell are poorly constrained, limiting the possibility to understand if solid-state convection can occur under Europa's ice shell conditions. To investigate how diurnal tidal flexing and the internal dynamics of Europa's ice shell influence the ice grain crystals' evolution, we adopted a thermal-mechanical numerical model that uses finite differences and marker-in-cell techniques, implementing the dynamic recrystallization of the ice and the ice grain evolution in a self-consistent way with the numerical model. We found that solid-state convection within Europa's ice shell can occur if it is diurnally tidally deformed, as the tidal stresses within the ice shell operate to reduce the ice grain sizes and the ice viscosity. We discuss future radio science experiments, in combination with radar sounder investigations, that will be capable of characterizing the possible presence of solid-state convection within Europa's ice shell.

1. Introduction

Since Voyager's observations of Europa's surface, it has been suggested that solid-state convection could occur within the outer ice shell (Consolmagno and Lewis, 1978; Reynolds and Cassen, 1979). The occurrence of surface geology on Europa such as chaotic terrains, pits, and domes (Pappalardo et al., 1998; Greeley et al., 1998) may be due to internal dynamics driven by convective motions within a thick outer ice shell (15–45 km, e.g., Sotin et al., 2002; Tobie et al., 2003; Showman and Han, 2004, 2005; Mitri and Showman, 2005), covering a global subsurface ocean, whose presence is indicated by the Galileo mission's induced magnetic field measurements (Kivelson et al., 2000). A further analysis of the Galileo spacecraft images suggests that a putative subduction-like convergent boundary may exist in Europa's ice shell providing possible evidence of a plate tectonic system driven by solid-state convection within the ice (Kattenhorn and Prockter, 2014). However, the presence of solid-state convection within the ice shell is still an open question and, in opposition to the solid-state convection hypothesis, a relatively thin (3–5 km thick) and conductive ice shell has been proposed to explain chaos terrain (Greenberg et al., 1999), and pit and dome formation (Greenberg et al., 2003).

Theoretical works have supported the hypothesis that solid-state convection could occur within Europa's outer ice shell. The effects of solid-state convection on Europa's ice shell have been numerically simulated using tidal heating (Sotin et al., 2002; Tobie et al., 2003; Showman and Han, 2004; Mitri and Showman, 2005; Han and Showman, 2011; Vilella et al., 2020) and the visco-elastic-plastic behaviour of the ice (Showman and Han, 2004, 2005). Numerical geodynamical models have previously investigated the influence of the grain-size-sensitive (GSS) creep (e.g., Sotin et al., 2002; Tobie et al., 2003; Showman and Han, 2004; Mitri and Showman, 2005) and the non-Newtonian behaviour of the ice on Europa's ice shell internal dynamics (Barr et al., 2004; Barr and Pappalardo, 2005; Freeman et al., 2006; Harel et al., 2020; Kalousová et al., 2016; Howell and Pappalardo, 2018). The grain-size-sensitive (GSS) diffusion creep is expected to be the dominant creep acting in a convective ice shell (e.g., Mitri and Showman, 2005) with a contribution to the deformation from the grain boundary sliding (Barr et al., 2004).

* Corresponding author at: International Research School of Planetary Sciences, Dipartimento di Ingegneria e Geologia, Università d'Annunzio, Viale Pindaro 42, Pescara 65127, Italy.
E-mail address: giuseppe.mitri@unich.it.

https://doi.org/10.1016/j.icarus.2023.115648
Received 15 July 2022; Received in revised form 22 May 2023; Accepted 25 May 2023
Available online 1 June 2023

The ice grain size within Europa's ice shell is poorly constrained, limiting our understanding if solid-state convection can occur under the physical conditions of Europa's ice shell. The ice grain size within Europa's ice shell is controlled by the ice crystals' growth rate and, simultaneously, by the ice crystals' size reduction rate under the stress originating from the internal dynamics of the ice shell. Previous numerical geodynamical models have assumed a homogeneous distribution of ice grain size within Europa's ice shell, considering de facto the ice grain size as a free parameter of the model and not modelling the ice grain evolution in a self-consistent way with the numerical model (e.g., Tobie et al., 2003; Showman and Han, 2004; Mitri and Showman, 2005; Harel et al., 2020). However, as discussed by Durham and Stern (2001), the ice grain size can be, in principle, constrained by modelling the physical conditions within the ice shell. In fact, it is expected that the ice dynamic recrystallization must bring a steady-state balance between the grain size reduction and the grain size growth. Barr and McKinnon (2007) have shown that the dynamic recrystallization of the ice, that is driven only by convective stresses within Europa's ice shell, could produce relatively large ice grain sizes (30–80 mm) within the convective sublayer of the ice shell, inhibiting any convective motions within the ice shell after a few convective overturns. Previously, McKinnon (1999) discussed that the dynamic recrystallization of the ice driven by the diurnal tidal flexing of the ice shell could decrease the ice grain size down to 1 mm, acting to stabilize solid-state convection within Europa's ice shell through time. However, the relationship between the tidal deformation and the onset of thermal convection within Europa's ice shell is still not well understood.

Terrestrial analogues and models based on cyclic loading experiments on ice suggest that dynamic recrystallization can occur at the expected low strain rate within Europa's ice shell. Analysis of the GReenland Ice core Project (GRIP) ice core, which has an inferred low strain rate of 2.5×10^{-12} s^{-1} (De La Chapelle et al., 1998) found that 650 m below the surface, the ice grains have ceased to grow reaching a steady state-grain size of ~4 mm (De La Chapelle et al., 1998). The cessation of ice grain growth is due to the nucleation of new grains and dislocations (De La Chapelle et al., 1998). De La Chapelle et al. (1998) found that for the GRIP ice the formation of sub-boundaries with the subdivision into two ice grains occurs every 2400 years and the generation of dislocations during this period is 1×10^{11} m^{-2}. At a lower strain rate, 2.3×10^{-13} s^{-1}, Vostok ice core analysis found that dislocation formation and dynamic recrystallization occurred (De La Chapelle et al., 1998). The presence of dislocation in ice in the presence of low strain rates in Greenland (GRIP and GISP 2, Greenland Ice Sheet Project 2) and Antarctic ice core samples show that dislocation processes and high dislocation densities do occur (De La Chapelle et al., 1998; Baker and Cullen, 2002; Cole, 2003). Modelling examining the linear relationship between anelastic strain and dislocation density (Cole, 1995) and experimental data based on the cyclic loading of ice found that a specimen with a value at or close to the freshwater value of porosity, like expected for Europa's ice shell, will have an initial dislocation density of 3×10^{8} m^{-2} (Cole, 1998; Cole and Durell, 2001). Cole and Durell (2001) show that the dislocation density evolves during straining as a function of stress, strain, and temperature considering the initial dislocation density such that the dislocation produced during deformation will be added together with the initial or pre-existing dislocations (Cole, 2004, 2020). Further the presence of impurities or particulate content could give rise to high dislocation densities regardless of deformation history (Cole, 2003).

We developed a numerical geodynamical model of the ice shell fully coupled with the ice grain evolution, modelling the ice dynamic recrystallization to simulate the steady-state ice grain size controlled by the ice crystals' growth and the ice crystals' size reduction under the stress originated from the convective motions and the tidal deformation within the ice shell. Due to the present lack of experimental data on ice for dynamic recrystallization (Durham and Stern, 2001), we have adopted the dynamic recrystallization analysis from De Bresser et al. (1998) on olivine which we use as a proxy for the dynamic recrystallization of ice, considering that the ice grain size reaches a steady-state grain size when the strain rate of the GSS grain boundary diffusion creep equals the contribution of the GSI dislocation creep.

2. Model

2.1. Equation of conservation of mass, momentum and energy

We model solid-state convection within Europa's ice shell solving the equations of conservation of mass, momentum and energy written as:

$$\nabla\cdot\vec{v} = 0 \tag{1}$$

$$\frac{\partial\sigma'_{xx}}{\partial x}+\frac{\partial\sigma'_{xy}}{\partial y}=\frac{\partial P}{\partial x} \tag{2}$$

$$\frac{\partial\sigma'_{yy}}{\partial y}+\frac{\partial\sigma'_{xy}}{\partial x}=\frac{\partial P}{\partial y}-\rho g \tag{3}$$

$$\rho c_p\left(\frac{\partial \mathrm{T}}{\partial t}+\vec{v}\cdot\nabla \mathrm{T}\right)=\frac{\partial}{\partial x}\left(k\frac{\partial T}{\partial x}\right)+\frac{\partial}{\partial y}\left(k\frac{\partial T}{\partial y}\right)+Q \tag{4}$$

The operator $\nabla\cdot$ indicates the divergence, $\vec{v}$ is the vector velocity defined by the components v_x and v_y in a two-dimensional Cartesian coordinate system with perpendicular horizontal x-axis and vertical y-axis. Adopting the Boussinesq approximation, the equations of conservation of mass are written as the continuity equation (Eq. (1)), assuming accordingly that $\nabla\cdot\vec{v}\gg\frac{1}{\rho}\frac{\partial\rho}{\partial t}$, where ρ is the fluid density and t is the time. The conservation of momentum is written in the form of the Navier-Stokes equations of the motion in a gravity field (Eqs. (2 and 3)), where σ'_{ij} are the deviatoric stresses, and i and j are the indexes of the coordinates, k is the thermal conductivity, P is the pressure, and g is the acceleration of gravity. The Navier-Stokes equations neglect the inertial forces of the viscous fluid. The conservation of the energy (Eq. (4)) considers an internal tidal heating source (Q). The operator $\nabla \equiv \left(\frac{\partial}{\partial x}, \frac{\partial}{\partial y}\right)$ is nabla, T is the temperature and c_p is the thermal heat capacity given by $c_p = k/\kappa\rho$, where κ is the thermal diffusivity and ρ is the density.

We adopt the numerical model developed by Gerya and Yuen (2003) to solve the differential equations of the conservation of mass, momentum, and energy, that use finite differences and marker-in-cell techniques, combining Lagrangian advecting markers with a Eulerian grid. Use of the marker-in-cell technique provides a way to solve advection problems with no diffusion of the material properties such as the petrological composition of a mantle. For this model assuming that the ice shell of Europa is water ice, a Eulerian instead of a Lagrangian method can be used to solve the advection equations. The differential eqs. 1–4 are solved in a two-dimensional rectangular geometry with a width:height ratio of 3:1. At the first time-step of the numerical simulations, a sinusoidal thermal perturbation and an ice grain size of 0.1 mm are imposed. The boundary conditions are free slip, where the normal component of the velocity vector on a domain boundary is zero and the orthogonal component does not change through the boundary. The temperature is fixed at the top and the bottom boundaries (see §2.2). The model mesh resolution is 70 × 140, and 200 × 600 randomly distributed markers.

2.2. Physical parameters

Following Vilella et al. (2020), the pressure dependence of the ice melting temperature is given by:

$$T_m = T_0\left(1-\frac{(P/10^6)}{395}\right)^{\frac{1}{9}} \tag{5}$$

Table 1
Model physical parameters (see Mitri and Showman, 2005).

Parameter	Symbol	Value/Relationship	Unit
Gravitational acceleration	g	1.32	m s^{-2}
Ice shell thickness	H	5–45	km
Thermal conductivity	k	Eq. (7)	W m^{-1} K^{-1}
Surface temperature	T_s	95	K
Bottom temperature	T_b	Eq. (5)	K
Ice thermal expansion	α	1.6×10^{-4}	K^{-1}
Ice thermal diffusivity	κ	1.3×10^{-6}	m^2 s^{-1}
Shear modulus	μ	4×10^9	Pa
Orbital frequency	ω	2×10^{-5}	s^{-1}

Table 2
Rheological parameters for dislocation creep.

Creep regime	log_{10}A (MPa^{-n} m^p s^{-1})	p	n	Q_{disl} (kJ mol^{-1})	References
Dislocation creep (T < 258 K)	5.1	0	4.0	61	Durham et al. (1992) Durham and Stern (2001)
Dislocation creep (T > 258 K)	28.8	0	4.0	181	Goldsby and Kohlstedt (2001)

where the lithostatic pressure is given by $P = \rho_0 g y$. We use Eq. (5) to compute both the temperature of the ice at the interface with the subsurface ocean and the liquidus curve within the ice shell. The density of the ice is modelled with a linear dependence on the temperature (T) given by (Feistel and Wagner, 2006):

$$\rho(T) = \rho_0(1 - \alpha(T - T_0)) \tag{6}$$

defined by a density of the ice at the temperature $T_0 = 273.15$ K equal to $\rho_0 = 916.72$ kg m^{-3}, where α is the thermal expansion of the ice. The temperature dependence of the thermal conductivity is given by (Slack, 1980):

$$k(T) = \frac{621}{T} \ [\mathrm{W\ m^{-1}}]. \tag{7}$$

The physical parameters of the model are summarized in Table 1.

2.3. Rheology and ice grain size

To model the time varying evolution of the ice grain size, we adopted the analysis by De Bresser et al. (1998) for the dynamic recrystallization of olivine, using experimental results on this mineral as a proxy for examining dynamic recrystallization of ice. As observed by De Bresser et al. (1998), steady-state grain size is achieved when the strain rate due to grain boundary diffusion creep of the grain size-sensitive (GSS) component ($\dot{\varepsilon}_{diff}$) equals the strain rate due to the dislocation creep of the grain size-insensitive (GSI) creep ($\dot{\varepsilon}_{disl}$). Following De Bresser et al. (1998), in our geodynamic model, we assumed grain boundary diffusion and dislocation creep for the ice dynamic recrystallization. We adopt the constitutive equation for the flow law that takes in account the grain size sensitive (GSS) diffusion creep (*diff*) and the grain size insensitive (GSI) dislocation creep (*disl*) (Goldsby and Kohlstedt, 2001):

$$\dot{\varepsilon}_{viscous} = \dot{\varepsilon}_{diff} + \dot{\varepsilon}_{disl} \tag{8}$$

We use for dislocation creep the flow law written as (Goldsby and Kohlstedt, 2001):

$$\dot{\varepsilon}_{disl} = A \frac{\sigma_d^n}{d^p} exp\left(-\frac{Q_{disl}}{RT}\right), \tag{9}$$

where A is a parameter, σ_d is the differential stress, n is the stress exponent, d is the ice grain size, p is the ice grain size exponent, Q_{disl} is the activation energy for creep and R is the gas constant (8.314 J mol^{-1} K^{-1}). Table 2 presents the adopted rheological data, including pre-melting rheological data, for dislocation creep obtained with compressive creep experiments using a molding cylinder and applying an axial stress (Durham et al., 1992; Goldsby and Kohlstedt, 2001; Durham and Stern, 2001). For dislocation creep, we write the flow law as $\dot{\varepsilon}_{disl} = \dot{\varepsilon}_{disl,c} + \dot{\varepsilon}_{disl,h}$ that simulates a smooth transition of the strain rate from cold to hot temperatures; considering for $\dot{\varepsilon}_{disl,c}$ the rheological parameters reported in Table 2 as $T < 258$ K (the subscript c is for cold), and for $\dot{\varepsilon}_{disl,h}$ the rheological parameters reported as $T > 258$ K (the subscript h is for hot).

We use an effective viscosity written as $\eta_{eff} = \sigma_{II}/2\dot{\varepsilon}_{II}$, where σ_{II} is the deviatoric stress and $\dot{\varepsilon}_{II}$is the deviatoric strain rate. For dislocation creep, the effective viscosity indicated with a caron symbol is written as (Gerya, 2009, p. 77):

$$\check{\eta}_{disl} = \frac{1}{2^{\frac{n-1}{n}} 3^{\frac{n+1}{2n}}} \frac{1}{A^{\frac{1}{n}} d^{\frac{p}{n}} \left(\dot{\varepsilon}_{II}\right)^{\frac{n-1}{n}}} exp\left(\frac{Q_{disl}}{nRT}\right) \tag{10}$$

For the grain size sensitive (GSS) creep, we adopt the grain boundary diffusion creep, also called the Coble creep, where the flow law is written as (Goldsby and Kohlstedt, 2001):

$$\dot{\varepsilon}_{diff,b} = \frac{14\sigma_d \Omega}{RTd^3} \pi \delta D_{0,b} exp\left(-\frac{Q_b}{RT}\right) \tag{11}$$

where $D_{0,b}$ is the grain boundary diffusion coefficient, Q_b is the activation energy for the grain boundary diffusion and δ is the grain boundary width. We adopt $D_{0,b} = 8.4 \times 10^{-4}$ m^2 s^{-1}, $Q_b = 49$ kJ mol^{-1} and $\delta = 9.04 \times 10^{-10}$ m (Goldsby and Kohlstedt, 2001). At low stress, the crystal deformation generally results in volume diffusion and grain boundary diffusion. The volume diffusion, with a dependence on the grain size as $\dot{\varepsilon}_{diff,v} \sim d^{-2}$, acts independently of the grain boundary diffusion, with a dependence on the grain size as $\dot{\varepsilon}_{diff,b} \sim d^{-3}$.

We write the equilibrium ice grain size due to the dynamic recrystallization (De Bresser et al., 1998; Durham and Stern, 2001):

$$d = \left(\frac{A_{GSS}}{A_{disl}}\right)^{\frac{1}{p}} exp\left(\frac{Q_{disl} - Q_{GSS}}{pRT}\right) \sigma^{-\frac{(n_{disl} - n_{GSS})}{p_{GSS}}} \tag{12}$$

where A_{GSS} and A_{disl} are constants derived from the flow law of grain size sensitive (GSS) creep (Eq. (11)) and grain size insensitive (GSI) dislocation creep (Eq. (9)), respectively, n_{GSS} and n_{disl} are the stress exponents of GSS and GSI creeps, p_{GSS} is the ice grain size exponent of GSI creep, and Q_{GSS} and Q_{disl} are the activation energies of GSS and GSI creeps. Observational evidence shows that the dynamic recrystallization presents a dependence between the grain size (d) and the stress (σ) as $d \propto \sigma^{-m}$, where the parameter $m \cong 1$ (De Bresser et al., 1998; Durham and Stern, 2001).

Modelling the evolution of the grain size with the mantle dynamics is challenging, as the grain size is influenced by the stress and, in turn, the rheology of the mantle depends on both the stress and the grain size. To model the ice grain size evolution within the ice shell we rely on the physical condition where the growth of the grain size is balanced by its reduction due to dynamic recrystallization. This results in a steady-state grain size that it is reached for the condition (De Bresser et al., 1998):

$$\dot{\varepsilon}_{disl} = \dot{\varepsilon}_{diff} \tag{13}$$

Using the flow law of the ice (Equation [8]) and the steady-state ice grain size condition (Eq. (13)), we write the constitutive equation for the ice flow law as:

$$\dot{\varepsilon}_{viscous} = 2\dot{\varepsilon}_{disl} \tag{14}$$

where the strain rate is twice the GSI dislocation creep strain rate (De Bresser et al., 1998; Durham and Stern, 2001). Our numerical model first

computes the viscosity as $\eta = \frac{1}{2}\eta_{disl}$, and then compute the steady-state ice grain size using Eq. (12). At the conclusion of each time cycle, the second strain rate invariant is computed resulting from the convective motions and from tidal deformation (see §2.4). The total second strain rate invariant is used to compute the viscosity for the subsequent time cycle.

2.4. Tidal deformation and heating

We model the tidal deformation of the ice shell using a Maxwell rheology (e.g., Tobie et al., 2003; Showman and Han, 2004; Mitri and Showman, 2005, 2008). The Maxwell rheology well describes the loading frequency viscoelastic behaviour of the ice, neglecting anelastic attenuation that would require a viscoelastic rheological model such as the Andrade rheology. During tidal cycling loading, the ice undergoes a repeating cycle of deformation and relaxation. The behaviour of a viscoelastic material to cycling loading with strain amplitude ε_0 can be modelled by solving a corresponding Hookean elastic problem in the complex domain (Biot, 1954; Tobie et al., 2005; Mitri and Showman, 2008). For the periodic tidal flexing of the ice shell given by $\sigma = \sigma_0 e^{i\omega t}$ and $\varepsilon = \varepsilon_0 e^{i\omega t}$, where σ_0 and ε_0 are the amplitude of the tidal stress tensor (σ) and strain tensor (ε), respectively, ω is the orbital frequency (2×10^{-5} s^{-1}), t is the time and $i^2 = -1$, we write the stress-strain relationship for a Maxwell rheology as $\sigma_0 = 2\tilde{\mu}\varepsilon_0$ (Mitri and Showman, 2008). The complex shear modulus is given by:

$$\tilde{\mu} = \frac{\omega^2\mu\eta^2}{\mu^2 + \omega^2\eta^2} + i\frac{\omega\mu^2\eta}{\mu^2 + \omega^2\eta^2} \tag{15}$$

where μ is the shear modulus (4×10^9 Pa). The temperature (T) dependent volumetric tidal heating is given by (Tobie et al., 2003; Mitri and Showman, 2005, 2008):

$$Q(T) = \omega\varepsilon_0^2\, Im(\tilde{\mu}) \tag{16}$$

We write the viscoelastic relationship between the tidal stress (σ_{tide}) and the amplitude of the tidal strain (ε_0) as:

$$\sigma_{tide} = 2\varepsilon_0 Re(\tilde{\mu}) \tag{17}$$

where ε_0 is the amplitude of the tidal strain of the ice shell. $Im(\tilde{\mu})$ and $Re(\tilde{\mu})$ denotes the imaginary and the real part of the complex shear modulus, respectively. The amplitude of the tidal strain of the ice shell is roughly estimated as $\varepsilon_0 \sim \xi/R$, where ξ is the amplitude of the vertical surface deformation during a tidal cycle (20–30 m; Moore and Schubert, 2000) and $R = 1569$ km is the mean radius of Europa, and it is estimated to range between 1×10^{-5} and 2×10^{-5} (Tobie et al., 2003; Showman and Han, 2004; Mitri and Showman, 2005, 2008). The viscosity η is computed as described in §2.3.

2.5. Internal melting

For self-consistency of the numerical model, we have characterized the melting condition of the ice. The fraction of internal melting rate is computed as:

$$\delta x_{melt} = \frac{c_p}{L}(T - T_m)\delta t^{-1} \tag{18}$$

where $c_p = k/\kappa\rho$ is the heat capacity, L is the latent heat of fusion (334 kJ kg^{-1}), T_m is the pressure dependent melting temperature computed using Eq. (5), and δt is the time step. In the presence of local partial melting, the density of the ice is computed taking in account the contribution of liquid water fraction, assuming a density of liquid water equal to 1000 kg m^{-3}. At each time step, when $T > T_m$, we impose the condition $T = T_m$.

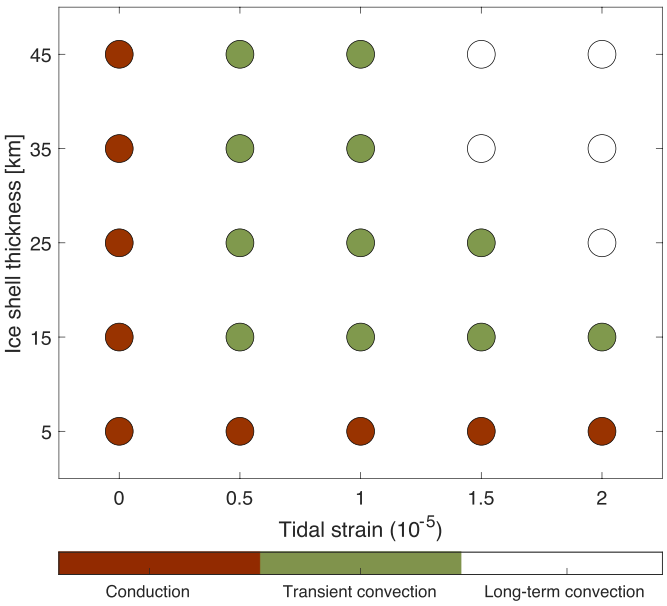

Fig. 1. Numerical simulation results on solid-state convection within Europa's ice shell exploring ice shell thicknesses in the 5 km – 45 km range and tidal strain in the 0–2.0 $\times$ 10^{-5} range. For each numerical simulation indicated as a circle, the occurrence of conduction is indicated in brown colour, transient-state convection is indicated in green colour, while long-term convection is indicated in white colour. (For interpretation of the references to colour in this figure legend, the reader is referred to the web version of this article.)

2.6. Gravity anomalies

We use the Bouguer gravity formula to compute the surface gravity anomaly produced by the simulated density distribution ($\rho(y)$) within the ice shell:

$$\Delta g_h = 2\pi G \int_0^h \rho(y)dy \tag{19}$$

where G is the universal gravitational constant (6.673×10^{-11} m^3 kg^{-1} s^{-2}). We use the milligal as the unit for the gravity anomaly, where 1 mGal is equal to 1×10^{-5} m s^{-2}.

3. Results

Our analysis highlights the importance of tidal deformation, in addition to the ice shell thickness, in determining the onset of solid-state convection. We first present the results of the numerical simulation to investigate the importance of the tidal strain, in addition to the ice shell thickness, on the thermal state of the ice shell. We then examine study cases to investigate the influence of the temperature, and tidal stress and convective stress on the ice grain reduction. We then present results that show the temporal evolution of the ice shell to elucidate the physical conditions to ensure the occurrence of convection. Finally, we discuss how the thermal structure of the ice shell can be investigated through radio science experiments.

3.1. Ice shell thickness and tidal strain

We performed 25 numerical simulations to explore how the ice dynamic recrystallization driven by tidal and internal dynamical stresses influences the physical conditions under which solid-state convection within Europa's ice shell can occur. The numerical simulations were run for ice shell thicknesses ranging between 5 km and 45 km (with 10 km intervals) and for tidal strain ranging between 0 and 2×10^{-5} (with 0.5 $\times$ 10^{-5} intervals). We adopted the ice shell thickness in the range

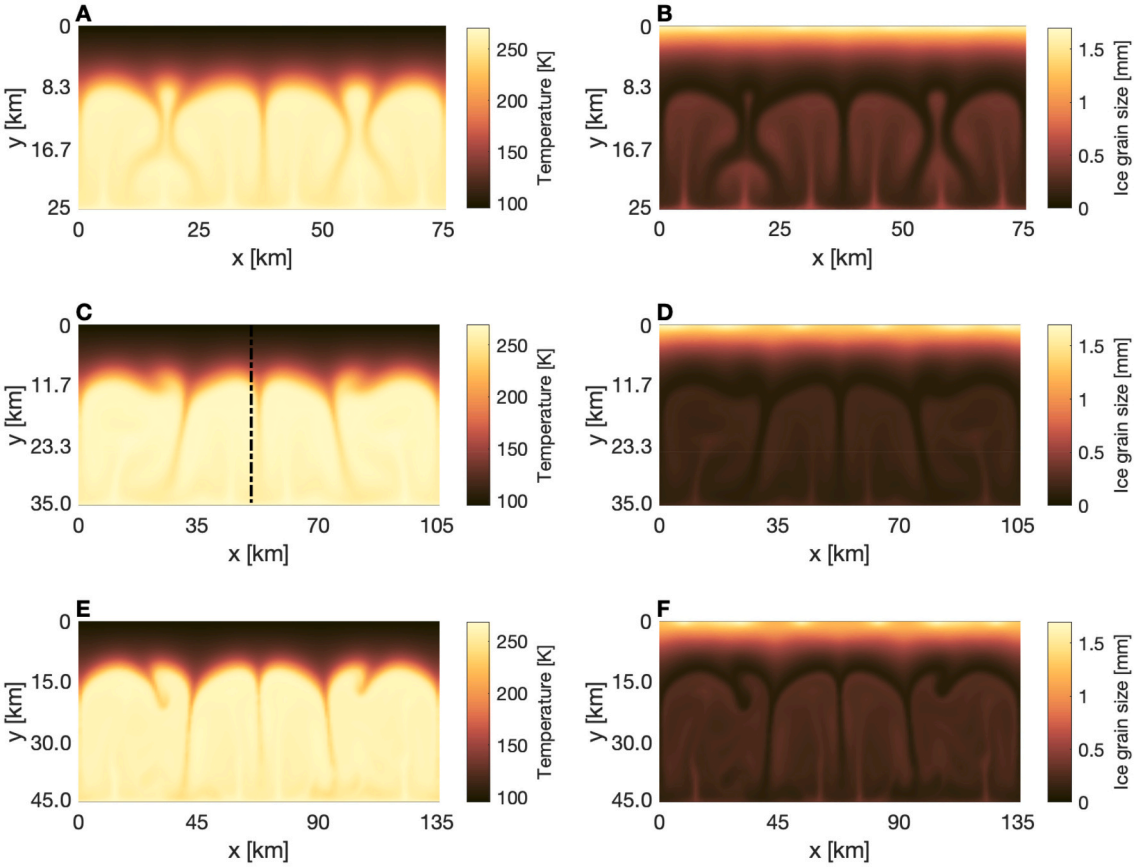

Fig. 2. Snapshot at 2.0×10^7 a of three numerical simulations of solid-state convection within Europa's ice shell. Panels A and B present the temperature and ice grain fields for an ice shell thickness H = 25 km; Panels C and D present the temperature and ice grain fields for H = 35 km; and Panels E and F present the temperature and ice grain fields for H = 45 km. The tidal strain is fixed at 2.0×10^{-5}. The dashed-dotted line in Panel C indicates the location of the temperature, stress and ice grain size profiles presented in Fig. 3.

estimated in previous studies (e.g., Williams and Greeley, 1998; Greenberg et al., 1999; Schenk, 2002; Tobie et al., 2003; Mitri and Showman, 2005).

Depending on the tidal strain amplitude, we found heat transport within Europa's ice shell can occur in two different regimes, in addition to the thermal conduction: long-term convection and transient-state convection. We define as long-term convection if thermal convection, after its onset, is steady over 2×10^7 a as simulated in the last time-step of the simulation. The selected time for the final iteration of the simulation has been chosen to be at least two orders of magnitude greater than the timescale of convective overturn (10^4–10^5 a). Instead, we define as transient-state convection if, after its onset, thermal convection experiences cessation during the simulation run and we find that the ice shell is in a conductive state at 2×10^7 a as simulated in the last time-step of the simulation. We verified the dynamic state of our simulations after 2×10^7 a, without necessarily achieving a convective steady-state solution. This approach allowed us to assess the state of our simulations without requiring additional computational resources and ensured that our results were representative of the convective behaviour over a sufficiently long period of time.

Fig. 1 summarizes the results of the numerical simulations, presenting for each numerical simulation denoted with a circle the occurrence of thermal conduction (in brown colour), transient-state convection (in green colour), and long-term convection (in white colour). For example, for an ice shell thickness $H = 5$ km, independent of the assumed tidal strain ($\varepsilon_0 = 0$–2.0×10^{-5}), the heat is transported through the ice shell by thermal conduction. For $H = 15$ km and in the absence of tidal stress ($\varepsilon_0 = 0$), the heat is transported through the ice shell by thermal conduction. For $H = 15$ km and tidal strain $\varepsilon_0 = 0.5 \times 10^{-5}$–$2.0 \times 10^{-5}$, the heat is transported through the ice shell by convection characterized by a transient-state regime. With the evolution of the simulation run, the ice shell with $H = 15$ km and $\varepsilon_0 = 0.5 \times 10^{-5}$–$2.0 \times 10^{-5}$ experiences the cessation of convection. For $H = 25$ km and $\varepsilon_0 = 0$, the heat is transported through the ice shell by thermal conduction. For $H = 25$ km and $\varepsilon_0 = 0.5 \times 10^{-5}$–$1.5 \times 10^{-5}$, the heat is transported by convection characterized by a transient-state regime. For $H = 25$ km and $\varepsilon_0 = 2.0 \times 10^{-5}$, the heat is transported by convection characterized by a long-term regime. For both $H = 35$ km and 45 km, and for both $\varepsilon_0 = 0.5 \times 10^{-5}$ and 1.0×10^{-5}, convection is in transient-state regime and for $\varepsilon_0 = 1.5 \times 10^{-5}$ and 2.0×10^{-5} convection is in a long-term regime.

Interestingly, our results show that the onset of solid-state convection within Europa's ice shell depends on two main parameters: the ice shell thickness, as discussed in previous works (Mitri and Showman, 2005), and the tidal strain. Our numerical simulations indicate that, with convective stress acting alone, the dynamic recrystallization of the ice is insufficient to reduce the grain sizes and the viscosity enough to support solid-state convection. This result is consistent with previous work by Barr and McKinnon (2007). The ice dynamic recrystallization driven principally by tidal stresses within Europa's ice shell acts to reduce the ice grain sizes and, consequently, the ice viscosity, allowing the onset of solid-state convection within the ice shell. Instead, for lower tidal stress, larger ice grain sizes and viscosity prevent the onset of convection. We found that, in absence of tidal stress, the low magnitude of the internal dynamical stresses produced by the convective motions alone produces large ice grains, preventing the onset of solid-state convection.

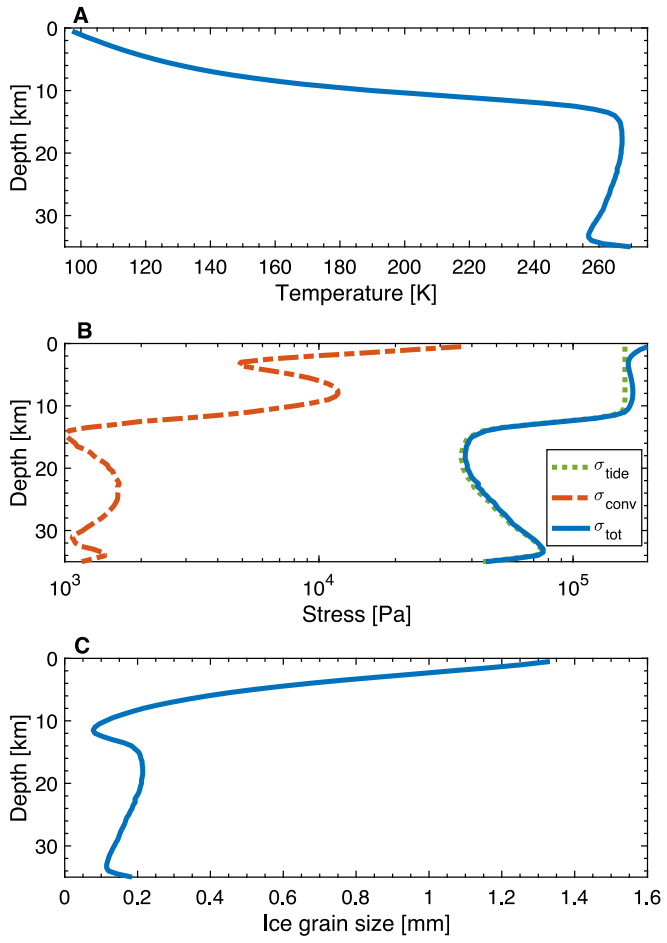

Fig. 3. Temperature, stress and ice grain size profiles, corresponding to a simulated upwelling for an ice shell thickness of 25 km and tidal strain of 2.0×10^{-5}. Panel A presents the temperature profile. Panel B presents the convective stress (brown lines), the tidal stress (green line), and the total stress given by the sum of the convective and tidal stress (blue lines), and Panel C presents the ice grain size profile. (For interpretation of the references to colour in this figure legend, the reader is referred to the web version of this article.)

3.2. Temperature, convective stress and tidal stress

We investigated how temperature and stress, including convective motion stress and tidal stress, influence the grain size of the ice. Specifically, we will first examine the effect of temperature and then of the stress on grain sizes, investigating how this influence the thermal state of the ice shell. Fig. 2 shows the snapshot at 2×10^7 a of three numerical simulations that were run for an ice shell thickness of 25 km, 35 km, and 45 km and for a fixed tidal strain of 2.0×10^{-5}. The left panels present the temperature fields and the right panels the ice grain size fields. For the physical conditions explored in the simulations presented in Fig. 2, internal melting was not found. The numerical simulations presented in Fig. 2 have been selected to show three case studies in which convective cells develop within the ice shell. A comparison between the temperature and grain size fields reveals that grain size within the ice shell is influenced by temperature, in addition to the stress. This temperature dependence is due to both the temperature dependence of the dynamic recrystallization model (Eq. (12)) and the viscoelastic response of the ice shell to the tidal deformation, which produces an upper region of the ice shell with an elastic behaviour characterized by the maximum magnitude of tidal stress and a lower region of the ice shell characterized by a viscous behaviour. The larger ice grain size occurs in the upper regions of the ice shell, where the temperature is lowest, even though the tidal stress is high. Within the viscous regions of the ice shell, the ice grain size in regions defined by cold descending plumes is lower with respect to the ice grain size of the hot ascending plumes.

We examine a case study to elucidate the influence of temperature, convective stress, and tidal stress on the ice grain size. Fig. 3 presents an example of temperature, stress profiles, and ice grain size profiles, corresponding to an upwelling of the numerical simulation with an ice shell thickness of 25 km and a tidal strain of 2.0×10^{-5}. Panel A of Fig. 3 shows the temperature profile, which is characteristic of stagnant lid convection with the formation of a stagnant lid in the shallower regions of the ice shell and a convective sublayer in the deeper regions. Panel B shows the convective stress (brown line), tidal stress (green line), and total stress given by the sum of the convective stress and the tidal stress (blue line). We note that the tidal stress is greater than convective stress, and we therefore expect the total stress that acts on dynamic recrystallization to be dominated by tidal stress rather than convective stress. Panel B also shows the viscoelastic response of the ice shell, where we observe the maximum stress in the shallower regions of the ice shell, where the ice shell behaves primarily as an elastic material. Instead, the stress decreases in the deeper regions of the ice shell, where the ice shell behaves primarily as a viscous material. Ice grain sizes depend on stress, both tidal and convective, as well as temperature. Panel C shows that in general the maximum ice grain size is reached in the shallower and colder region of the ice shell, while there is a decrease in ice grain size in the deeper and warmer regions of the ice shell, even if the stresses are lower with respect to the shallower regions.

We examine case studies to elucidate the influence of the ice shell thickness and the tidal strain amplitude on the ice grain size within the ice shell. Fig. 4 presents the mean temperature, stress, viscosity and ice grain size profiles for an ice shell thickness of 35 km and tidal strain of 1.0×10^{-5} (panels A1 – A4), 1.5×10^{-5} (panels B1 – B4), and 2.0×10^{-5} (panels C1 – C4). Fig. 4 also presents the mean temperature, stress, viscosity and ice grain size profiles for an ice shell thickness of 45 km and tidal strain of 0.5×10^{-5} (panels D1 – D4), 1.0×10^{-5} (panels E1 – E4), 1.5×10^{-5} (panels F1 – F4), and 2.0×10^{-5} (panels G1 – G4). The results simulations include cases with conductive thermal transport, characterized by the temperature profiles in panels A1, D1, and E1, and cases with solid-state convection, characterized by the temperature profiles in panels B1, C1, F1, and G1. The temperature profile in panel E1 corresponds to a subcritical state near the onset of convection. In the conductive cases, the average stresses shown in panels A2 and D2 indicate an elastic response of the ice shell, with a constant stress throughout the ice shell. In contrast, in the subcritical case, we observe a variation in stress within the ice shell (panel E2). Additionally, in the conductive cases the viscosity decreases within the ice shell depth (panels A3, D3, and E3), with higher viscosity in shallower regions with respect to deeper regions of the ice shell. In the convective cases, the stresses within the ice shell show a viscoelastic response, with higher stresses in shallower regions where the ice shell behaves primarily as an elastic material, and lower stresses in deeper regions, where the ice shell behaves primarily as a viscous material (panels B3, C3, F3, and G3). The average viscosity profile is of particular interest, as the Rayleigh number depends inversely on the viscosity. Increasing the tidal strain amplitude decreases the average viscosity within the ice shell, promoting convection. This can be observed by comparing panels D3, E3, F3, and G3, where increasing the tidal strain amplitude from 0.5×10^{-5} to 2.0×10^{-5} results in a decrease in viscosity within the ice shell. Finally, the ice grain size depends on the tidal strain, which is influenced by temperature and viscoelastic stress response. In general, increasing the tidal strain amplitude results in a decrease in ice grain size. This can be observed in panels D4, E4, F4, and G4, where increasing the tidal strain amplitude from 0.5×10^{-5} to 2.0×10^{-5} results in a decreasing ice grain size in shallower regions of the ice shell, while the ice grain size remains almost constant with submillimeter size in deeper regions.

Now we elucidate the evolution of the ice shell thermal state and its dependence on mean ice grain size, considering two numerical simulations with an ice shell thickness of 35 km, varying the tidal strain

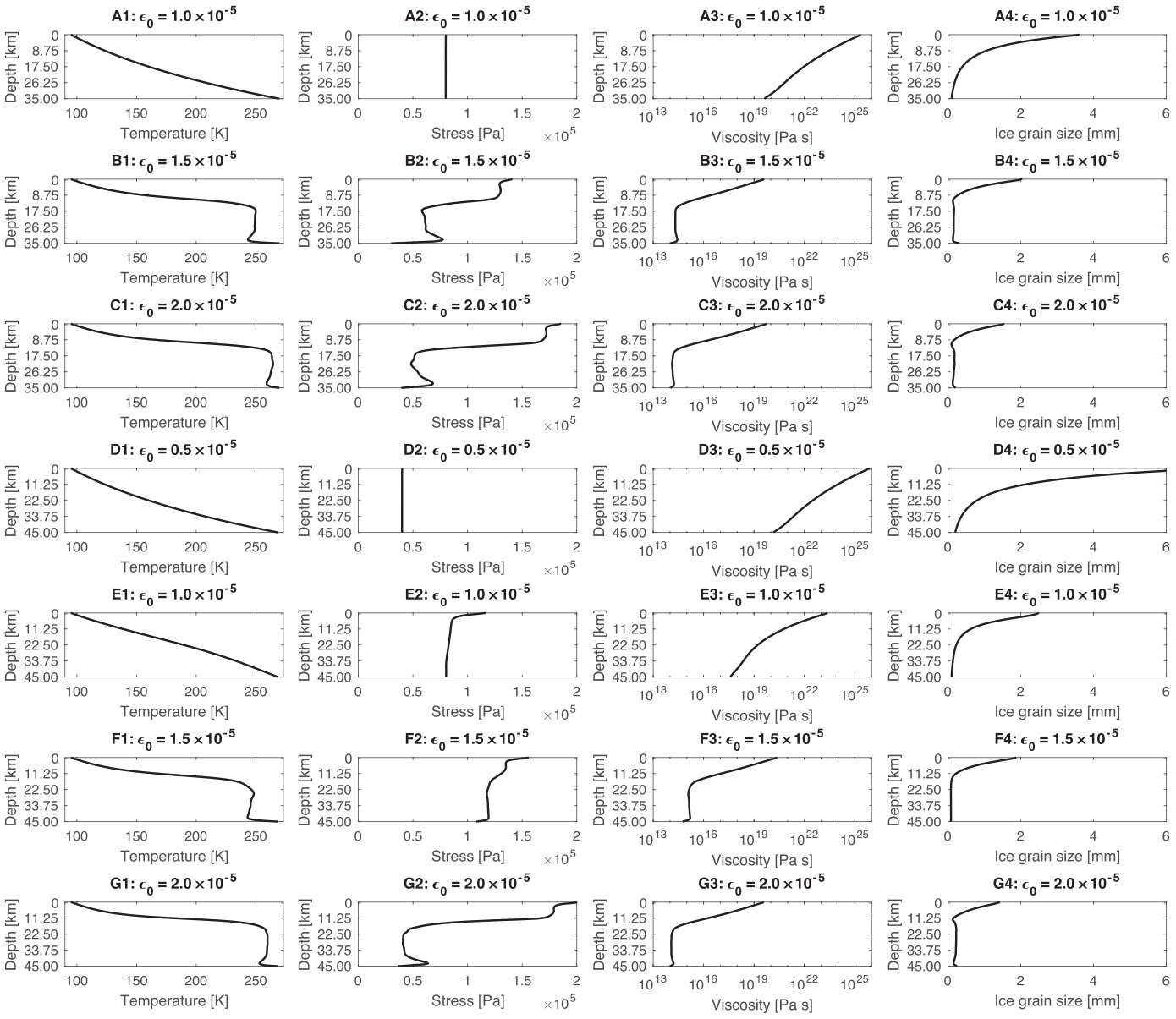

Fig. 4. Mean temperature, stress, viscosity and ice grain size profiles for an ice shell thickness of 35 km and tidal strain of 1.0×10^{-5} (panels A1 – A4), 1.5×10^{-5} (panels B1 – B4), 2.0×10^{-5} (panels C1 – C4), and for an ice shell thickness of 45 km and tidal strain of 0.5×10^{-5} (panels D1 – D4), 1.0×10^{-5} (panels E1 – E4), 1.5×10^{-5} (panels F1 – F4), 2.0×10^{-5} (panels G1 – G4).

amplitude. Fig. 5 presents the time-step evolution of the non-dimensional root mean square (rsm) velocity, and mean ice grain size for two different tidal strain amplitude values: 1.0×10^{-5} and 1.5×10^{-5}. The two simulations correspond to the cases of transient-state convection and long-term convection. We first examine the case of transient-state convection. During the time-step evolution, after the onset of convection the non-dimensional root mean square velocity and convective motions cease (Panel A), approaching zero. Panel B shows the mean ice grain size within the ice shell is approximately 0.58 mm during the long-term convection. After the cessation of convection, the mean ice grain size increases to approximately 0.80 mm. In contrast, for a tidal strain amplitude of 1.5×10^{-5}, convection motions within the ice shell are always present, as demonstrated by the analysis of the non-dimensional root mean square velocity, which remains >106. In this case, the mean ice grain size within the ice shell is approximately 0.39 mm.

3.3. Gravity anomalies

We present results that show the potential for investigating the thermal structure of Europa's ice shell using radio science data to measure the gravity field. The internal temperature variations with the ice shell resulting from the formation of convective cells give rise to density variations that produce gravity anomalies. We quantify the gravity anomalies resulting from thermal convection in the ice shell for several case studies. Conversely, we do not expect to observe gravity anomalies resulting from a conductive thermal structure of the ice shell. Fig. 6 shows the gravity anomalies produced by the density variations due to the occurrence of convective motions within Europa's ice shell. Fig. 6 presents the gravity anomalies results for long-term convection for an ice shell thickness $H = 45$ km and tidal strain $\varepsilon_0 = 1.5 \times 10^{-5}$ (Panel A), $H = 45$ km and $\varepsilon_0 = 2.0 \times 10^{-5}$ (Panel B), H = 35 km and $\varepsilon_0 = 1.5 \times 10^{-5}$ (Panel C), $H = 35$ km and $\varepsilon_0 = 2.0 \times 10^{-5}$ (Panel D), and $H = 25$ km and $\varepsilon_0 = 2.0 \times 10^{-5}$ (Panel E). The maximum predicted gravity anomalies within a convective ice shell are found for $H = 45$ km and $\varepsilon_0 = 2.0$

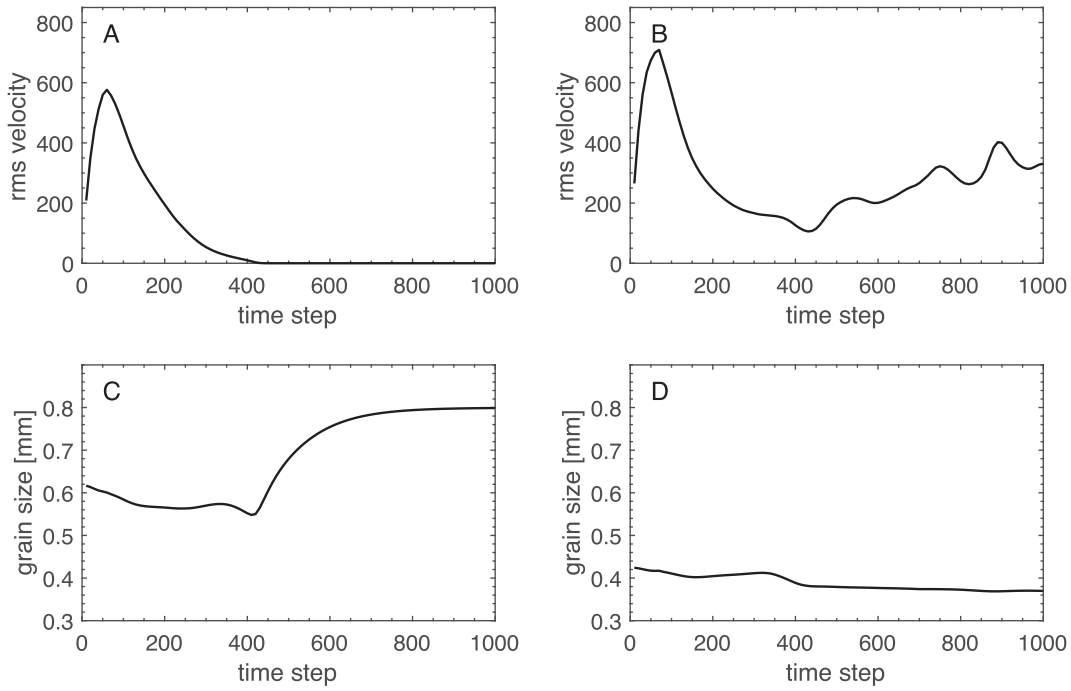

Fig. 5. Non-dimensional root mean square (rms) velocity and ice grain size for an ice shell thickness of 35 km and tidal strain of 1.0×10^{-5} (panels A, and B), and 1.5×10^{-5} (panels B, and D).

$\times 10^{-5}$, corresponding to 8.8 mGal. In general, larger ice shell thicknesses produce larger gravity anomalies within a convective ice shell.

Fig. 7 shows the snapshot at 0.2×10^{7} a of a numerical simulation that was run for an ice shell thickness of 45 km and for a fixed tidal strain of 1.0×10^{-5}. Panel A presents the temperature field, Panel B the ice grain fields, and Panel C the resulting gravity anomalies. The numerical simulation results presented in Fig. 7 correspond to the transient-state convection (see Fig. 1), where after the onset of convection, the ice shell experiences the cessation of the convection. The snapshot at 0.2×10^{7} presents the thermal plumes that are still developing within the ice shell. The maximum predicted gravity anomalies within the convective ice shell are 7.4 mGal.

4. Discussion

We investigated how diurnal tidal flexing and internal dynamics of Europa's ice shell influences the ice crystals' evolution for the 0–45 km ice shell thickness range and the 0–2×10^{-5} tidal strain range and, consequently, the onset of solid-state convection, and its stability through the time, implementing a numerical geodynamical code that consistently models the evolution of the ice grain size. McKinnon (1999) had previously discussed how the diurnal tidal flexing of Europa's ice shell should affect the mean ice grain size, reaching an equilibrium grain size within a convective sublayer on the order of 1 mm. For a mean ice grain size of 1 mm, and assuming grain boundary sliding creep and a tidal strain rate of 2×10^{-10} s^{-1}, McKinnon (1999) estimated that solid-state convection can occur within Europa's ice shell for thicknesses larger than 25 km. McKinnon (1999) has also shown that a reduction of the ice grain sizes facilitates the development of solid-state convection within a thinner Europan ice shell up to a thickness of ~10 km for an ice grain size of 0.1 mm. Assuming an initial convective state for the ice shell, Barr and McKinnon (2007) have shown that within a convecting ice shell formed of ice without impurities, the ice crystals which evolution is influenced only by the stress generated by the convective motions, without tidal stress, must reach an equilibrium grain size ranging between 30 and 80 mm, increasing the ice viscosity and, consequently, inhibiting any convective motions within the ice shell after a few convective overturns. Barr and McKinnon (2007) have remarked that impurities within the ice can reduce the ice grains, making the convective motions possible within the ice shell.

We have investigated for the first time the influence of tidal stress on the onset of convection within the ice shell of Europa with a numerical geodynamical model, previously explored by McKinnon (1999) adopting an analytical method, in combination with internal dynamical stress previously explored by Barr and McKinnon (2007). The advantage of a numerical geodynamical method with respect to an analytical method is its capability to model in a self-consistent way the viscous-elastic response of the ice shell and the ice grain size evolution. Our numerical simulations show that the dynamic recrystallization driven by the diurnal tidal flexing of Europa's ice shell, in combination with stresses generated by the convective motions within the ice, act to reduce the ice grain sizes, confirming the previous study results by McKinnon (1999). We found that if the ice shell is experiencing only internal stress generated by convective motions, then ice grains evolve rapidly, inhibiting the onset of convection, as previously described by Barr and McKinnon (2007). We conclude that the diurnal tidal flexing of the ice shell, reducing the ice grain size, is a driving process for the onset of solid-state convection within Europa's ice shell. We found that the ice grain size distribution is heterogeneous within a convective ice shell, as the dynamic recrystallization of the ice grains depends on the applied stress and the temperature. The influence of the impurities within the ice on the dynamic recrystallization has not been investigated in this study. However, the presence of impurities favours the ice grain size reduction with respect to the ice without impurities (Azuma et al., 2012), and therefore the presence of impurities could produce lower ice grain sizes with respect to our numerical simulation results, facilitating the onset of solid-state convection within the ice shell with respect to the case of pure water ice.

Based on our numerical simulation results, we argue that the geological activity triggered by the solid-state convection within the ice shell could be strongly influenced by the ice grain size reduction driven by the diurnal tidal flexing of the ice. Interestingly, as the amplitude of the tidal stresses are expected to change through time due to the orbital evolution of Europa, likely in response to the orbital Laplace resonance

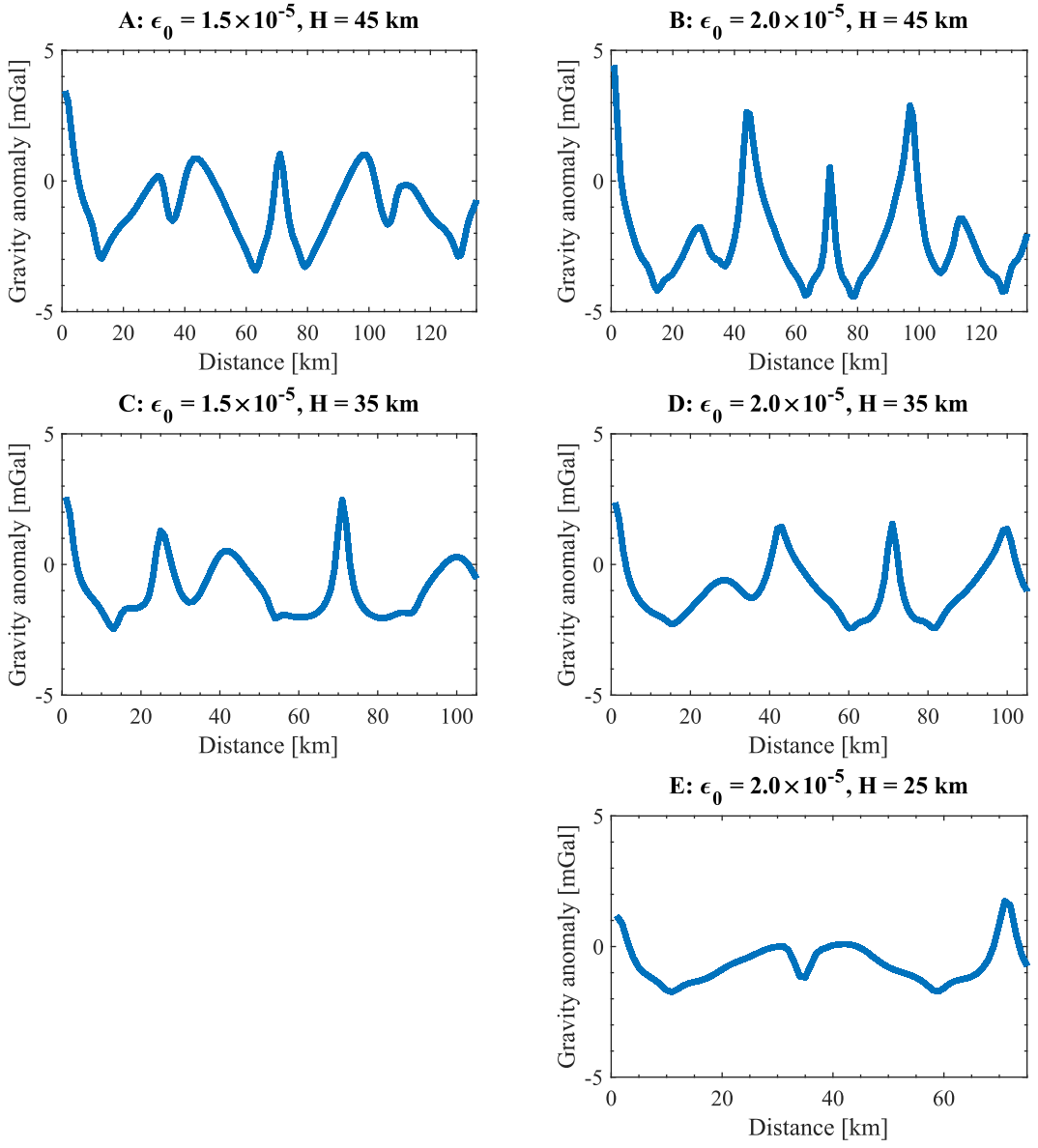

Fig. 6. Gravity anomalies for long-term convection for an ice shell thickness H = 45 km and tidal strain $\varepsilon_0 = 1.5 \times 10^{-5}$ (Panel A), H = 45 km and $\varepsilon_0 = 2.0 \times 10^{-5}$ (Panel B), H = 35 km and $\varepsilon_0 = 1.5 \times 10^{-5}$ (Panel C), H = 35 km and $\varepsilon_0 = 2.0 \times 10^{-5}$ (Panel D), and H = 25 km and $\varepsilon_0 = 2.0 \times 10^{-5}$ (Panel E).

evolution (Malhotra, 1991), the periods of geological activity, due to the onset of solid-state convection within the ice shell can be manifested as episodic events related to the periods for which the tidal stresses are enough high to reduce the ice grain size to critical values. When the diurnal tidal flexing is low, the ice grain growth within the ice shell inhibits the solid-state convection and the ice shell could transit to a conductive state. Differently, an ice shell in a conductive state that experiences an increase in tidal flexing with associated ice grain size reduction, because of the reduction in viscosity, can experience the onset of solid-state convection within the ice shell. Depending on the tidal strain magnitude, we found that convection within Europa's ice shell can occur both in a long-term convective regime and a transient-state convective regime. If the tidal strain is higher than 1.5×10^{-5} and the ice shell thickness is >35 km, and if the tidal strain is higher than 2.0×10^{-5} and the ice shell thickness is >25 km, then convection is expected to occur in a long-term regime where, successively from the onset of the convection, the convection within the ice shell is stable. Instead, in the case of a lower strain rate and lower ice shell thickness, convection is expected to occur in the transient-state regime where, after the onset of convection and the development of thermal plumes, the ice shell experiences the cessation of the convection, overturning the ice shell in a conductive state. For the parameters herein explored, we found that the transient-state regime can occur if the tidal strain is higher than 0.5×10^{-5} and if the ice shell thickness is higher than 15 km. In addition to tidal stress as investigated in this study, internal stresses produced by libration (Sarid et al., 2006), ice shell thickness variations (Nimmo, 2004; Mitri and Showman, 2005), non-synchronous rotation (McEwen, 1986; Leith and McKinnon, 1996; Geissler et al., 1998) or true polar wander (Leith and McKinnon, 1996; Schenk et al., 2008) could also influence the dynamic recrystallization of the ice and, potentially, the onset of solid-state convection within the ice shell.

The purpose of this study is to develop a numerical geodynamical model that can simulate the possible effects of tidal deformation on the onset of thermal convection within Europa's ice shell. However, due to the lack of experimental data on ice, it is unclear which creep to use for the dynamic recrystallization of ice. To address this issue, we used experimental data from De Bresser et al. (1998) for olivine as a proxy for dynamic recrystallization in ice. This data suggests that the dynamic

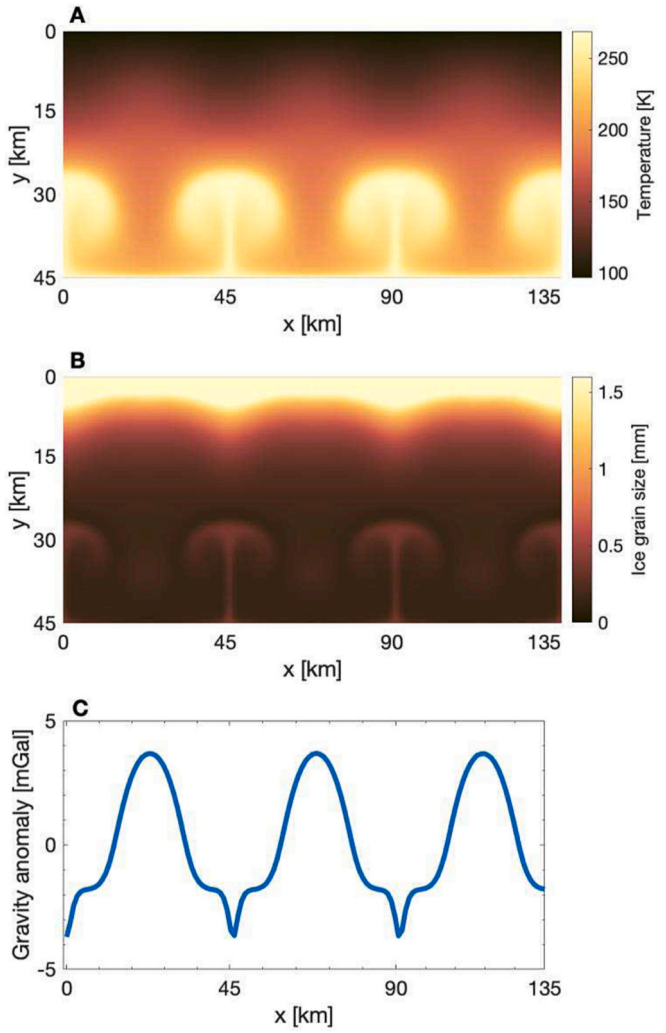

Fig. 7. Snapshot at 0.2×10^7 a of numerical simulations of transient-state convection within Europa's ice shell for an ice shell thickness of 45 km and a tidal strain 1.0×10^{-5}. Panel A presents the temperature field, Panel B the ice grain fields, and Panel C the gravity anomalies.

recrystallization reaches a steady-state grain size when the strain rate of grain size sensitive (GSS) grain boundary diffusion creep equals the contribution of the strain rate of the grain size insensitive (GSI) dislocation creep. Although this approach provides useful insights, it is important to note that ice may behave differently from olivine and that a combination of different creeps might be possible. Future laboratory experiments on dynamic recrystallization in ice could clarify the contribution of different creeps and improve the accuracy of our theoretical predictions for Europa's ice shell.

We used the rheological analysis derived from Goldsby and Kohlstedt (2001)'s compressive creep experiments, where a molding cylinder is used to apply axial stress to ice samples, to study the behaviour of Europa's ice shell under both convective and tidal stress. Under tidal stress, Europa's ice shell also experiences cyclic loading in addition to convective stress. Cyclic loading with zero-mean-stress experiments by Cole and Durell (2001) have shown that the stress exponent, n, is dependent on the dislocation density. When the applied stress increases the dislocation density, the value of n is compatible with the dislocation creep, whereas n is compatible with the diffusion creep when the dislocation density remains constant during straining. These results obtained with cyclic loading with zero-mean-stress experiments are in line with the rheological behaviour of ice observed in compressive creep experiments (Goldsby and Kohlstedt, 2001). Although uncertainties may exist in applying the rheological model obtained from compressive creep experiments to cyclic loading conditions, which are relevant to modelling the tidal flexing of Europa's ice shell, it provides a useful proxy for understanding ice rheology behaviour under these conditions.

The tidal strain amplitude on Europa's ice shell varies depending on the location, with the mean tidal strain amplitude over the entire surface of Europa's ice shell expected to be approximately half the peak value. Our numerical simulations investigate the influence of tidal strain amplitude from 0 to 2×10^{-5}, encompassing the possible values within Europa's ice shell. Our study highlights the potential importance of tidal deformation as a mechanism for driving convective processes within Europa's ice shell. However, the local interaction between tidal deformation and convective processes is more complex than explored in this study, which assumed a constant value of the tidal strain amplitude. A three-dimensional treatment of the tidal strain amplitude and the coupling between tidal deformation and convective processes is needed to refine our understanding of this mechanism's importance in the context of Europa's ice shell.

The radar sounder called Radar for Europa Assessment and Sounding: Ocean to Near-surface (REASON), with operating frequencies of 9 MHz and 60 MHz, that will be on board the spacecraft (S/C) of the Europa Clipper mission and the radar sounder called Radar for Icy Moon Exploration (RIME), with an operating frequency of 9 MHz, that will be on board of the S/C of the Jupiter Icy moon Explorer (JUICE) mission will both investigate the structure of Europa's ice shell, including the thermal structure potentially describing the transition from the stagnant lid and the convective sublayer, the geometries of the thermal plumes and cold downwelling, and the internal melts (Bruzzone et al., 2013, 2015; Di Paolo et al., 2016; Blankenship et al., 2018). Di Paolo et al. (2016) have estimated that the RIME instrument will characterize the structure of Europa's ice shell down to 12–15 km from the surface. We propose that, in combination with radar sounder investigations, radio science experiments could characterize the gravity anomalies produced by the internal density variations due to the thermal structure of Europa's ice shell, including the wavelength of the convective structures. Koh et al. (2022) have modelled possible sources of gravity anomalies on Europa produced at degree-2 both from the rotational and tidal deformation of the outer ice shell and the rocky deep interior, and at higher degrees from the surface and the basal topography of the outer ice shell, and the seafloor topography of the deep rocky interior. Koh et al. (2022), in agreement with previous works (Pauer et al., 2010), found that the seafloor topography could dominate the gravity field up to degree 22, while the gravity field signals from the outer ice shell is distinguishable at higher degrees. Koh et al. (2022) have estimated that the long-wavelength ice shell thickness variation could produce a gravity anomaly of ~3.4 mGal. The Bouguer gravity anomaly, corrected for the gravity anomaly contribution of short-wavelength surface topography, could highlight the gravity contribution of the internal structure of the outer ice shell, including the thermal structure of a convective ice shell at high degrees. Our numerical simulations estimate that the larger gravity anomalies produced by the thermal structure of a convective ice shell is 8.8 mGal that it is higher than the expected long-wavelength ice shell thickness variation gravity field signal. The radio science experiment with a spatial resolution higher than a few tens degrees is a suitable technique that could be used in future missions to investigate the thermal structure of Europa. However, the gravity field of Europa will be measured from the upcoming Europa Clipper mission up to degree 10 (Mazarico et al., 2021) and at lower degrees from JUICE mission (Parisi et al., 2014).

5. Conclusions

The presence of solid-state convection within the ice shell is still an open question and, in opposition to the solid-state convection hypothesis (e.g., Sotin et al., 2002; Tobie et al., 2003; Showman and Han, 2004; Mitri and Showman, 2005), a relatively thin (3–5 km thick) and

conductive ice shell has been proposed to explain chaos terrain (Greenberg et al., 1999), and pit and dome formation (Greenberg et al., 2003). The ice grain size is considered a fundamental free parameter that was adopted in previous numerical simulations that were aiming to describe the internal dynamics of Europa's ice shell and to define the physical conditions necessary to have solid-state convection within Europa's ice shell. We have shown that, in fact, the ice grain size is not a free parameter and, in principle, can be estimated. Our numerical simulations show that the presence of convection within the ice shell is directly related to the magnitude of tidal strain that Europa is experiencing. We also found that if Europa's ice shell is not tidally deformed, then the ice grain growth inhibits solid-state convection, and the ice shell is in a conductive state. We have argued that, depending on the tidal strain magnitude, convection within Europa's ice shell can occur in both a long-term convective regime and a transient-state convective regime, and that the geological activity of Europa could be directly related to episodic events where convection is present within the ice shell. Future investigations using data from radar sounder instruments and, as we proposed, in conjunction with radio science experiments will be capable of characterizing the thermal structure of Europa's ice shell and the possible presence of solid-state convection.

Declaration of Competing Interest

None.

Data availability

Data will be made available on request.

Acknowledgements

G.M. acknowledges support from the Italian Space Agency (2023-6-HH.0). The author thanks three anonymous reviewers for useful comments. The scientific colour map lajolla (Crameri, 2018) is used in this study.

References

Azuma, N., Miyakoshi, T., Yokoyama, S., Takata, M., 2012. Impeding effect of air bubbles on normal grain growth of ice. J. Struct. Geol. 42, 184–193.
Baker, I., Cullen, D., 2002. The structure and chemistry of 94 m Greenland ice sheet project 2 ice. Ann. Glaciol. 35, 224–230.
Barr, A.C., McKinnon, W.B., 2007. Convection in ice I shells and mantles with self-consistent grain size. J. Geophys. Res.: Planet. 112 (E2).
Barr, A.C., Pappalardo, R.T., 2005. Onset of convection in the icy Galilean satellites: influence of rheology. J. Geophys. Res. 110, E12005. https://doi.org/10.1029/2004JE002371.
Barr, A.C., Pappalardo, R.T., Zhong, S., 2004. Convective instability in ice I with non-Newtonian rheology: application to the icy Galilean satellites. J. Geophys. Res. 109, E12008. https://doi.org/10.1029/2004JE002296.
Biot, M.A., 1954. Theory of stress-strain relations in anisotropic viscoelasticity and relaxation phenomena. J. Appl. Phys. 25 (11), 1385–1391.
Blankenship, D., Ray, T., Plaut, J., Moussessian, A., Patterson, W., Romero-Wolf, A., Grima, C., Young, D., Soderlund, K., Gim, Y., Schroeder, D., 2018. REASON for Europa. 42nd Cospar Scientific Assembly, 42. B5–B3.
Bruzzone, L., et al., 2013. RIME: Radar for icy moon exploration. In: 2013 IEEE International Geoscience and Remote Sensing Symposium-IGARSS. IEEE, pp. 3907–3910.
Bruzzone, L., et al., 2015. Jupiter ICY moon explorer (JUICE): Advances in the design of the radar for Icy Moons (RIME). In: 2015 IEEE International Geoscience and Remote Sensing Symposium (IGARSS). IEEE, pp. 1257–1260.
Cole, D.M., 1995. A model for the anelastic straining of saline ice subjected to cyclic loading. Philosoph. Magaz. A 72 (1), 231–248.
Cole, D.M., 1998. Modeling the cyclic loading response of sea ice. Int. J. Solids Struct. 35 (31−32), 4067–4075.
Cole, D.M., 2003. A dislocation-based analysis of the creep of granular ice: preliminary experiments and modeling. Ann. Glaciol. 37, 18–22.
Cole, D.M., 2004. A dislocation-based model for creep recovery in ice. Philos. Mag. 84 (30), 3217–3234.
Cole, D.M., 2020. On the physical basis for the creep of ice: the high temperature regime. J. Glaciol. 66 (257), 401–414.
Cole, D.M., Durell, G.D., 2001. A dislocation-based analysis of strain history effects in ice. Philosoph. Magaz. A 81 (7), 1849–1872.
Consolmagno, G.J., Lewis, J.S., 1978. The evolution of icy satellite interiors and surfaces. Icarus 34, 280–293.
Crameri, F., 2018. Scientific colour maps. Zenodo 10. https://doi.org/10.5281/zenodo.1243862.
De Bresser, J.H.P., Peach, C.J., Reijs, J.P.J., Spiers, C.J., 1998. On dynamic recrystallization during solid-state flow: effects of stress and tem- perature. Geophys. Res. Lett. 25, 3457–3460.
De La Chapelle, S., Castelnau, O., Lipenkov, V., Duval, P., 1998. Dynamic recrystallization and texture development in ice as revealed by the study of deep ice cores in Antarctica and Greenland. J. Geophys. Res. Solid Earth 103 (B3), 5091–5105.
Di Paolo, F., et al., 2016. Radar signal penetration and horizons detection on Europa through numerical simulations. IEEE J. Select. Top. Appl. Earth Observat. Remote Sens. 10 (1), 118–129.
Durham, W.B., Stern, L.A., 2001. Rheological properties of water ice-applications to satellites of the outer planets. Annu. Rev. Earth Planet. Sci. 29 (1), 295–330.
Durham, W.B., Kirby, S.H., Stern, L.A., 1992. Effects of dispersed particulates on the rheology of water ice at planetary conditions. J. Geophys. Res.: Planet. 97 (E12), 20883–20897.
Feistel, R., Wagner, W., 2006. A new equation of state for H2O ice Ih. J. Phys. Chem. Ref. Data 35 (2), 1021–1047.
Freeman, J., Moresi, L., May, D.A., 2006. Thermal convection with a water ice I rheology: implications for icy satellite evolution. Icarus 180 (1), 251–264.
Geissler, P.E., Greenberg, R., Hoppa, G., Helfenstein, P., McEwen, A., Pappalardo, R., Tufts, R., Ockert-Bell, M., Sullivan, R., Greeley, R., Belton, M.J.S., 1998. Evidence for non- synchronous rotation of Europa. Nature 391 (6665), 368–370.
Gerya, T., 2009. Introduction to Numerical Geodynamic Modelling. Cambridge University Press.
Gerya, T.V., Yuen, D.A., 2003. Characteristics-based marker-in-cell method with conservative finite-differences schemes for modeling geological flows with strongly variable transport properties. Phys. Earth Planet. Inter. 140 (4), 293–318.
Goldsby, D.L., Kohlstedt, D.L., 2001. Superplastic deformation of ice: experimental observations. J. Geophys. Res. Solid Earth 106 (B6), 11017–11030.
Greeley, R., Sullivan, R., Klemaszewski, J., Head III, J.W., Pappalardo, R.T., et al., 1998. Europa: Initial Galileo geological observations. Icarus 135, 4–24.
Greenberg, R., Hoppa, G.V., Tufts, B.R., Geissler, P., Riley, J., Kadel, S., 1999. Chaos on Europa. Icarus 141, 263–286.
Greenberg, R., Leake, M.A., Hoppa, G.V., Tufts, B.R., 2003. Pits and uplifts on Europa. Icarus 161, 102–126.
Han, L., Showman, A.P., 2011. Coupled convection and tidal dissipation in Europa's ice shell using non-Newtonian grain-size-sensitive (GSS) creep rheology. Icarus 212 (1), 262–267.
Harel, L., Dumoulin, C., Choblet, G., Tobie, G., Besserer, J., 2020. Scaling of heat transfer in stagnant lid convection for the outer shell of icy moons: influence of rheology. Icarus 338, 113448.
Howell, S.M., Pappalardo, R.T., 2018. Band formation and ocean- surface interaction on Europa and Ganymede. Geophys. Res. Lett. 45 (10), 4701–4709.
Kalousová, K., Souček, O., Tobie, G., Choblet, G., Čadek, O., 2016. Water generation and transport below Europa's strike- slip faults. J. Geophys. Res.: Planet. 121 (12), 2444–2462.
Kattenhorn, S.A., Prockter, L.M., 2014. Evidence for subduction in the ice shell of Europa. Nat. Geosci. 7 (10), 762–767.
Kivelson, M.G., Khurana, K.K., Russell, C.T., Volwerk, M., Walker, R.J., Zimmer, C., 2000. Galileo magnetometer measurements: a stronger case for a subsurface ocean at Europa. Science 289, 1340–1343.
Koh, Z.W., Nimmo, F., Lunine, J.I., Mazarico, E., Dombard, A.J., 2022. Assessing the detectability of Europa's seafloor topography from Europa Clipper's gravity data. Planet. Sci. J. 3 (8), 197.
Leith, A.C., McKinnon, W.B., 1996. Is there evidence for polar wander on Europa? Icarus 120, 387–398.
Malhotra, R., 1991. Tidal origin of the Laplace resonance and the resurfacing of Ganymede. Icarus 94 (2), 399–412.
Mazarico, E., Buccino, D.R., Castillo-Rogez, J., Dombard, A., Genova, A., Hussmann, H., Kiefer, W., Lunine, J., McKinnon, W., Nimmo, F., Park, R.S., 2021. The Europa clipper gravity/radio science investigation. LPSC 52, 1784.
McEwen, A.S., 1986. Tidal reorientation and fracturing on Jupiter's moon Europa. Nature 321, 49–51.
McKinnon, W.B., 1999. Convective instability in Europa's floating ice shell. Geophys. Res. Lett. 26 (7), 951–954.
Mitri, G., Showman, A.P., 2005. Convective–conductive transitions and sensitivity of a convecting ice shell to perturbations in heat flux and tidal-heating rate: implications for Europa. Icarus 177 (2), 447–460.
Mitri, G., Showman, A.P., 2008. A model for the temperature-dependence of tidal dissipation in convective plumes on icy satellites: implications for Europa and Enceladus. Icarus 195 (2), 758–764.
Moore, W.B., Schubert, G., 2000. The tidal response of Europa. Icarus 147, 317–319.
Nimmo, F., 2004. Stresses generated in cooling viscoelastic ice shells: application to Europa. J. Geophys. Res. 109, E12001.
Pappalardo, R.T., et al., 1998. Geological evidence for solid-state convection in Europa's ice shell. Nature 391 (365–368), 1998.
Parisi, M., Iess, L., Finocchiaro, S., 2014. The gravity fields of Ganymede, Callisto and Europa: how well can JUICE do. Geophys. Res. Abstr. EGU 2014 (16), 11758.
Pauer, M., Musiol, S., Breuer, D., 2010. Gravity signals on Europa from silicate shell density variations. J. Geophys. Res.: Planet. 115 (E12).
Reynolds, R.T., Cassen, P.M., 1979. On the internal structure of the major satellites of the outer planets. Geophys. Res. Lett. 6, 121–124.

Sarid, A.R., Greenberg, R., Hurford, T.A., 2006. Crack azimuths on Europa: sequencing of the northern leading hemisphere. J. Geophys. Res. 111, E08004.
Schenk, P.M., 2002. Thickness constraints on the icy shells of the Galilean satellites from a comparison of crater shaper. Nature 417, 419–421.
Schenk, P.M., Matsuyama, I., Nimmo, F., 2008. True polar wander on Europa from global-scale small-circle depressions. Nature 453, 368–371.
Showman, A.P., Han, L., 2004. Numerical simulations of convection in Europa's ice shell: implications for surface features. J. Geophys. Res. E01010.
Showman, A.P., Han, L., 2005. Effects of plasticity on con- vection in an ice shell: implications for Europa. Icarus 177, 425–437.
Slack, G.A., 1980. Thermal conductivity of ice. Phys. Rev. B 22, 3065–3071.
Sotin, C., Head, J.W., Tobie, G., 2002. Europa: tidal heating of upwelling thermal plumes and the origin of lenticulae and chaos melting. Geophys. Res. Lett. 29, 1233.
Tobie, G., Choblet, G., Sotin, C., 2003. Tidally heated convection: constraints on Europa's ice shell thickness. J. Geophys. Res. 108, 5124.
Tobie, G., Mocquet, A., Sotin, C., 2005. Tidal dissipation within large icy satellites: applications to Europa and titan. Icarus 177 (2), 534–549.
Vilella, K., Choblet, G., Tsao, W.E., Deschamps, F., 2020. Tidally heated convection and the occurrence of melting in icy satellites: application to Europa. J. Geophys. Res.: Planet. 125 (3) e2019JE006248.
Williams, K.K., Greeley, R., 1998. Estimates of ice thickness in the Conamara Chaos region of Europa. Geophys. Res. Lett. 25, 4273–4276.